Elastic recovery in roll compaction simulation

Hannah L. Keizer, Peter Kleinebudde*

Heinrich Heine University Düsseldorf, Institute of Pharmaceutics and Biopharmaceutics Universitätsstraße 1, 40225 Düsseldorf, Germany

ABSTRACT

Roll compaction/dry granulation is a widely used granulation method in the pharmaceutical industry. The simulation of the process is of great interest, especially in the early phase of formulation development of solid dosage forms. The hybrid modeling approach allows to predict the roll compaction process parameters to produce ribbons with a desired solid fraction. Based on the process parameters, compacts (ribblets) of the same solid fraction are produced on a single punch press. So far, the prediction accuracy for the solid fraction of the ribbons was not satisfactory. It was found that the lack in prediction accuracy was due to the elastic recovery, which was not considered in the model. In this study, the fast in-die and the slow out-of-die elastic recovery of different excipients with varying compaction properties were investigated. A method was established to compensate for the elastic recovery of compacts in roll compaction simulation and to improve the prediction accuracy of the solid fraction considerably. The results were successfully implemented into the model through an additional learning step. Moreover, the findings were transferred to the mimicking of an API containing formulation. By modeling, it was possible to accurately predict the process settings to obtain ribbons with the desired solid fraction using only a small amount of material.

1. Introduction

Roll compaction/dry granulation is an often-used dry granulation method in the pharmaceutical industry. The aim of the granulation step is amongst others to improve the flowability of the powder blend by particle enlargement, to lower the dust generation and to reduce the bulk volume in order to optimize the tableting process and to ensure a good content uniformity of the final tablets. An advantage of the dry granulation process is its applicability to heat and/or moisture sensitive materials, since the usage of liquid binders and a drying step are omitted. The process has gained in interest, also because it is suitable for continuous production lines. Leane et al. (2015) range the roll compaction process after direct compression at second place in their manufacturing classification system for oral solid dosage forms.

The poorly flowing powder blend is densified with a certain specific compaction force between two counter-rotating rolls into intermediate compacts called ribbons, which are subsequently milled into granules. Depending on the chosen process parameters – specific compaction force (SCF), gap width (GW) and roll speed (RS) - more or less dense ribbons are produced. Their solid fraction (SF) is decisive for the resulting granule strength and granule size distribution as well as for the tensile strength of the final tablets (Sun and Kleinebudde, 2016). The roll compaction process can be divided into three zones (Guigon and Simon, 2003). First, the feeding zone. It is characterized by low stresses and mainly particle rearrangement takes place in this zone. The roll peripheral velocity is higher compared to the one of the powder, which slips on the roll surface. Second, the compaction zone. The compaction zone is described by the nip angle. This is the angle at the point of the transition between slip and non-slip of the powder on the roll surface and the powder is dragged in between the rolls. In this zone, the powder is compacted to ribbons depending on the used materials by either plastic flow and/or particle fragmentation and creation of new bonding areas. Third, the extrusion zone. After passing through the minimum gap width, the formed ribbons exit the rolls and undergo elastic recovery after the release of pressure.

Elastic recovery is a well-known and widely investigated phenomenon in the field of tableting. According to Train (1956), the tableting process on the particle level can be divided into four stages. After forming a denser powder bed by slipping of the particles (stage 1) and the formation of temporary columns and vaults (stage 2), structural failure of the material occurs under fragmentation or plastic flow (stage 3). In stage 4, the voids of the porous compact further decrease and a structure of sufficient strength is formed. In the decompression phase, the tablet volume increases due to elastic recovery, which continues after ejection. Depending on material properties like the yield pressure, the indentation hardness and the elasticity, pharmaceutical powders

---

show a predominant compression behaviour of fragmentation, plastic flow and/or elastic deformation (Roberts and Rowe, 1987). Antikainen and Yliruusi (2003) state that all materials show a more or less pronounced plastic and elastic part during compression, differing in their extent. Elastic recovery can be divided into two parts, the fast in-die elastic recovery and the slow out-of-die elastic recovery. For some materials, the elastic recovery can continue even for several hours or days after compaction (Picker, 2001). Several materials were tested and the in-die and out-of-die elastic recovery of the tablets at varying solid fractions was compared. The different extent of elastic recovery and the observed time dependencies were linked to the material properties. Maarschalk et al. (1997) stated that stress relaxation of tablets after compression can manifest itself as tablet expansion and/or capping. A direct relation between the stored energy within the tablet and the volume expansion was found. High bonding capacities of powder combined with a high stored energy and a high ejection friction coefficient favour capping of the tablets. On the other hand, low bonding strengths combined with low ejection friction coefficients lead to tablets with low resistance towards an increase in compact volume and thus an increase in porosity. Mazel et al. (2013) implemented a method to link the elastic moduli with the total elastic recovery of the compacts. Nevertheless, an instrumented die to measure the radial stresses is necessary. Katz et al. (2013) developed a method to characterize a material regarding its compression behaviour including the (visco-)elastic recovery in- and out-of-die with only one compression cycle. It was assumed first, that the elastic recovery after decompression is equal to the increase in SF during the elastic deformation under pressure and second, that the elastic recovery is independent of the maximum pressure applied. Antikainen and Yliruusi (2003) on the opposite showed that there is a pressure dependency of the elastic recovery. They established an elasticity factor to characterize the elastic recovery in the decompression phase and implemented a method to quantify the pressure dependency of elastic recovery. Paronen and Juslin (1983) used the differences between in-die and out-die Heckel plots to characterize the fast and slow elastic behaviour of starches. Ilic et al. (2013) compared the deformation behaviour of pharmaceutical powders using in-die and out-of-die methods based on the Heckel and Walker equations. It was found that the in-die analysis falsely suggests better compressibility than the out-of-die methods, since the elastic deformation is not considered in the in-die analysis. Furthermore, they suggested to use out-of-die methods, since they provide a more realistic picture of the properties of the final tablets.

The phenomenon of elastic recovery can be transferred from die compression to roll compaction. When ribbons exit the gap between the rolls, they undergo an elastic recovery. This results in ribbons thicker than the set GW what is accompanied by a reduction in the ribbon SF compared to the powder under load (Patel et al., 2010). Mahmah et al. (2019) investigated the phenomenon of longitudinal and transverse ribbon splitting in roll compaction and linked it with the elastic recovery of the ribbons. A splitting index was introduced in analogy to the capping index for tabletting (Akseli et al., 2013), that correlates the elastic recovery at a certain maximum roll stress with the ribbon tensile strength. Nkansah et al. (2008) introduced a method for the estimation of ribbon solid fraction by using the compaction throughput and included a correction factor that compensates for the relaxation after compaction.

The interest of simulating the roll compaction process is great, especially in the early phase of formulation development of solid dosage forms, because only a limited amount of API is available. Several approaches have been introduced over time but the number of literature taking into account the elastic recovery of the ribbons is limited. Johansons (1965) one-dimensional rolling theory of granular solids may be the best-known approach and was often modified to improve its prediction capabilities. 2D finite element modeling was used by several authors (Cunningham, 2005; Dec et al., 2003; Michrafy et al., 2011; Muliadi et al., 2012) in order to extend Johansons method and to

predict in addition to the roll pressure distribution and the nip angle also the occurring two-dimensional shear stresses and material velocity gradients. In all studies, the ribbon density was calculated at the gap but the extrusion zone and elastic recovery of the ribbons was not part of the modeling. Zinchuk et al. (2004) introduced the simulation of the roll compaction process with a uniaxial compaction simulator. Tensile strength and solid fraction served as comparative quality attributes for real and simulated ribbons. The amount of material needed to conduct the roll compaction feasibility experiments was reduced considerably. Bi et al. (2014) investigated if the Johanson model can correctly predict the maximum roll surface pressure. It was found that the predicted maximum roll surface pressure is much higher than the one used on the tableting machine to obtain compacts with the same solid fraction. These differences were attributed to the powder velocity gradients occurring during roll compaction, which are not considered by Johanson. A roll force and gap insensitive but material dependent mass correction factor was established to take into account the correct material throughput and it was possible to predict the maximum roll surface pressure. Nesarikar et al. (2012a) used instrumented rolls to measure the normal roll stresses and developed statistical models to link the mean ribbon density with the maximum normal stress and the gap width using out-of-die porosity – compression pressure profiles obtained by analysis of the pre-blend on a compaction simulator. In a further study (Nesarikar et al., 2012b), a placebo model based on a calibrated Johanson equation was developed to predict ribbon density for an API containing formulation and to facilitate the scale-up process. The approaches result in good prediction of ribbon relative density but instrumented rolls, which are necessary for the model calibration, are not always available. Reynolds et al. (2010) highlighted the importance of the roll compaction model input parameters material compressibility and the pre-consolidation relative density for the outcome of the prediction. Values estimated from the roll compaction process itself were compared with those from uniaxial compaction. The differences were attributed to the elastic recovery, which is taken into account in the measurements of the ribbon relative density after roll compaction, but not in the in-die measurements of the uniaxial compaction. It was concluded that the parameters estimated by uniaxial compaction would over-predict the ribbon density and model input data were taken from the roll compaction experiments. This leads to an accurate ribbon density prediction but with the drawback of high material consumption for the preliminary roll compaction experiments. Peter et al. (2010) developed the thin layer model to predict the density and force in roll compaction. To calculate the corresponding compaction pressure, the forces along the roll surface are summed up. Here, forces occurring during the compaction phase are considered as well as the forces during the extrusion phase. Nevertheless, the model takes into account only SF calculated at the gap by a throughput method and does not consider the elastic recovery of the compacts which takes place after leaving the compaction zone. Toson et al. (2019) highlighted that most of the mechanistic models do not use the final ribbon solid fraction but the solid fraction at gap. They established an iterative calibration of the compression coefficients in low throughput roll compaction experiments. They predicted the throughput and the final ribbon solid fraction with an in-silico DoE taking into account the elastic recovery. Nevertheless, compared to other modeling approaches the material consumption for the preliminary roll compaction experiments is relatively high.

The hybrid modeling approach used in this study is a further development of the thin layer model (Peter et al., 2010). Hybrid modeling is an easy to use approach for simulating and mimicking the roll compaction process with the uniaxial compaction simulator Styl'One Evolution (Medelpharm, France) using only a small amount of material and was described in detail by Reimer and Kleinebudde (2019). With this method, rectangular compacts (called ribblets) with the same SF as real ribbons from roll compaction can be produced. To do so, the most relevant roll compaction parameters - SCF, GW and RS – are mimicked

Table 1
Powder characteristics of excipients (mean ± SD) *mean of different batches.

Material	Powder density [g/cm^3]	Bulk density [g/cm^3]	Tapped density [g/cm^3]	Residual moisture [%]
MCC	1.5513 ± 0.305*	0.329 ± 0.005	0.437 ± 0.004	4.75 ± 0.36
DCPA	2.8555 ± 0.317	0.725 ± 0.003	0.842 ± 0.003	0.89 ± 0.17
Lactose	1.5439 ± 0.227	0.615 ± 0.004	0.711 ± 0.005	0.68 ± 0.12
Carrageenan	1.7332 ± 0.215	/	/	12.56 ± 0.48
HPMC	1.3017 ± 0.203	/	/	3.32 ± 0.67

on the uniaxial compaction simulator. An experimentally determined material independent correction factor is applied, which is specific for the mimicked roll compactor. It compensates for hardly imitable parameters like the feeding system or the roll design to find the correct compression pressure that corresponds to the SCF on the roll compactor. It is evident that simulation and mimicking on a uniaxial compaction simulator cannot cover all important parameters of the roll compaction process. This includes the feeding system, the inhomogeneous density distribution within the ribbons due to powder velocity gradients and powder feeding patterns due to the rotational movement of the screw and the fraction of fines. Nevertheless, Zinchuk et al. (2004) have hypothesised, that real and simulated ribbons with the same tensile strengths have the same mechanical properties decisive for the subsequent milling step. It was found, that the tensile strengths for real and simulated ribbons with the same solid fraction are equivalent. Furthermore, they concluded that the shear forces occurring during roll compaction process but not in die compression do not lead to relevant differences in the mechanical properties. For the hybrid modeling approach, it was shown that it is possible to produce ribblets with the same average SF as ribbons from roll compaction (Reimer and Kleinebudde, 2019). Thus, the simulation and mimicking with a uniaxial system are considered suitable to correctly mirror the roll compaction process. However, the prediction accuracy for the SF was not sufficient for the tested materials. The predicted ribblet SFs were often higher than the actual ones, especially for microcrystalline cellulose. It was assumed that the lack of prediction accuracy was due to the elastic recovery of the compacts because the resulting volume expansion was not included into the hybrid modeling calculations (Reimer and Kleinebudde, 2019).

In this study, the elastic recovery of different materials after compaction shall be evaluated. The extent of elastic recovery - in-die and out-of-die - shall be measured with regard to its dependence on the compression pressure, compression speed and powder bed thickness/ gap width. The aim of this study was to consider the elastic recovery inside and outside of the die in the hybrid modeling approach to allow an accurate prediction of the final ribblet and ribbon solid fraction. Finally, roll compaction of an ibuprofen containing formulation shall be mimicked to show the applicability of the approach to a formulation compared to the so far tested pure excipients MCC and lactose in a previous study (Reimer and Kleinebudde, 2019).

2. Materials and methods

2.1. Materials

Several pharmaceutical excipients were used in this study which are characterized by different compaction behaviours and varying degrees of elastic recovery after compaction. Two predominantly plastically deforming cellulose derivatives were used, microcrystalline cellulose (Vivapur 102, JRS Pharma) and hypromellose (HPMC, Pharmacoat 603, 3 mPa*s, substitution type 2910, Shin Etsu). Anhydrous alpha lactose (Tablettose 80, Meggle) and dibasic calcium phosphate (DiCaFos A150, Budenheim) were chosen as brittle materials. Carrageenan (Gelcarin GP 812, FMC Biopolymer) was used as a material showing a distinct elastic behaviour. The materials were stored under controlled conditions (21 °C, 45% RH) for at least one week to allow equilibration.

The mimicked formulation contains 20% (w/w) ibuprofen 50 (BASF), 75.8% (w/w) mannitol (Parteck M200, Merck), 4% (w/w) crospovidone (Polyplasdone XL, Ashland) and 0.2% (w/w) sodium lauryl sulfate (Stepanol 100, Stepan Company). Magnesium stearate (Ligamed MF-2-V, Peter Greven) was used for external lubrication.

2.2. Characterisation of starting materials

The starting materials were characterised regarding their powder true, bulk and tapped density and residual moisture. All measurements were performed in triplicate. The results are given as mean values with standard deviations in Table 1.

The powder density was determined with a helium pycnometer (AccuPyc 1330, Micromeritics). A 3.5 cm^3 chamber was used, ten purge cycles and five measurement cycles were performed per run. The temperature was kept constant at 25 °C ± 1 °C.

The bulk and tapped densities of the materials were determined according to method 2.9.34 of the European Pharmacopoeia.

The measurement of the excipients residual moisture was carried out with an infrared balance (MA 10D, Sartorius, Germany). The measurement was performed at 105 °C and was terminated as soon as the balance detected a change in moisture less than 0.1%/min.

2.3. Roll compaction

The roll compaction experiments were performed on a Mini-Pactor (Gerteis Maschinen + Processengineering AG, Switzerland). A rim roll sealing system and rolls with a diameter of 25 cm, 2.5 cm width and smooth surface were used. The automatic gap control was activated so that the powder quantity necessary to obtain the desired GW was controlled by the speed of the feeding screw. The tamping to feeding screw speed ratio was set at 160% and the roll speed was set at 2 rpm. Ribbon samples were collected one minute at steady-state conditions (GW ± 0.1 mm, SCF ± 0.1 kN/cm). Full factorial experimental designs with two factors at various levels and three repetitions at the centre point were used to produce the MCC and DCPA ribbons (Table 2). The process parameters were recorded with a frequency of 1 Hz.

Table 2
Roll compaction experimental design.

Material	SCF [kN/cm]	GW [mm]	Centre Point
MCC	3, 3.5, 4, 4.5, 5, 6, 7, 8, 9, 10, 11, 12, 13, 14, 15, 16, 17, 18	2, 4	9 kN/cm, 3 mm
DCPA	3, 5, 7, 9, 11, 13, 15, 17	2, 4	11 kN/cm, 3 mm

2.4. Hybrid modeling of roll compaction

The roll compaction process on a Mini-Pactor was mimicked with the hybrid modeling approach on the uniaxial compaction simulator Styl'One Evolution (Medelpharm, France). The method is described in literature (Reimer and Kleinebudde, 2019) and is based on the thin layer model (Peter et al., 2010). It is summarised in the following.

Hybrid modeling consists of two parts. One part is a mathematical model, which converts the applied compression pressure from the uniaxial compaction experiments to the SCF on the roll compactor. It divides the powder bed into thin layers and considers the occurring forces during the compression and as well during the decompression cycle. To convert the compression pressure into the correct SCF, a material independent conversion factor is needed which was found to be 0.667 for the Gerteis Mini-Pactor (Reimer and Kleinebudde, 2019).

The second part is a mechanical mimicking of the roll compaction process, in which rectangular flat faced punches represent the smooth roll surface. The minimal distance between upper and lower punch mimics the GW. The punches sine shaped displacement and speed represent the roll movement. The resulting compacts (called ribblets) mimic the ribbons and show the same SF.

Two learning phases are performed during the simulation. These learning phases are used for the determination of the compression behaviour of the tested materials by creating pressure-density profiles at different filling depths at a constant force of 51 kN (255 MPa). The mass of the learning tablets is measured on an analytical balance and is saved in the ANALIS software of the Styl'One. Based on the desired GW and the compression pressure a second learning is performed at an adapted filling depth to refine the simulation of the SCF.

The predicted corresponding SF is displayed. It is calculated by the punch dimensions (10 × 20 mm) and the minimum distance between upper and lower punch according to Eq. (1).

$$SF_{ribblet} = \frac{\frac{m}{h_{min} \times l \times w}}{\rho_{powder}} \times 100 \tag{1}$$

where m is the mass, h_{min} the minimum distance between the punches during compaction, l the length of the punch, w the width of the punch and ρ_{powder} the powder density of the starting material.

During the learning phases and the production, the die can be filled either by a feed shoe or by hand depending on the flowability of the material as well as on the available amount of material. External lubrication can be used to avoid ejection forces above the safety threshold of 2000 N. The lubricant is sprayed automatically in powder form onto the punches and into the die by compressed air (3–4 bar) for 500 ms each time before a tablet is compressed. The external lubrication unit was used to produce lactose and DCPA compacts as well as for the ibuprofen containing formulation.

2.5. In-die elastic recovery

Five excipients (MCC, lactose, DCPA, Carrageenan, HPMC) were tested regarding their in-die elastic recovery dependent on the applied compression pressure. The occurring forces and the punch positions during the compression cycle are monitored by piezo electric force sensors and displacement transducers (resolution: 1 μm; accuracy: ± 5 μm). To measure the fast elastic recovery in-die, the distance between the punches is taken where the force on the upper punch decreases to zero (Fig. 1). This corresponds to the separation of the upper punch in its upward movement from the surface of the compact after its in-die recovery. The elastic recovery in-die ($ER_{in\text{-}die}$) is calculated according to Eq. (2) which is based on the equation introduced by Armstrong and Haines-Nutt (1972).

$$ER_{in-die} = \frac{(h_{ZF} - h_{min})}{h_{min}} \times 100 \tag{2}$$

where h_{min} is the minimum distance between the upper and the lower punch during the compression and h_{ZF} the distance between the punches at zero force on the upper punch during its upward movement.

2.5.1. Influence of mimicked roll speed and the dwell time on the elastic recovery

To investigate the influence of the compression speed on the fast in-die elastic recovery of MCC, the mimicked RS was varied between 3 and 11 rpm (3, 5, 7, 9 and 11 rpm). The experiments were performed at a constant GW of 3 mm and a constant SCF of 6 kN/cm that corresponds to a compression pressure of 32 MPa. Ten ribblets were produced for each setting.

The influence of the dwell time on the elastic recovery was tested by using the "extended dwell time" tableting cycle of the Styl'One. Dwell times between 600 and 3000 ms were applied. Dwell time is defined as the time period, in which the maximum force on upper and lower punch is held constant. The punch positions changed slightly under maximum force due to the occurring material creep. A compression height of 3 mm was set and the resulting force was 3.5 kN (17.5 MPa) at its peak. Ten compacts were produced for each dwell time setting.

2.6. Out-of-die elastic recovery

2.6.1. Confocal chromatic measurement of out-of-die elastic recovery

Compacts of pure MCC, lactose and Carrageenan were produced at five compression pressures between 50 and 250 MPa on the Styl'One Evolution. The powder was filled to the die manually, the 10 × 20 mm flat faced punch and the default "one compression cycle" of the Styl'One were used to form the compacts. To produce lactose compacts, the die was lubricated with magnesium stearate to avoid too high ejection forces.

The slow out-of-die elastic recovery which takes place after ejection of the compact was measured over a time period of 30 min with a chromatic confocal probe (CHRocodile E, Precitec Optronik GmbH). These measurements were performed two times per compaction pressure setting.

The light of the white light source is directed to the optical probe which creates a full spectrum of light. The probe focuses the light of different wave lengths on the surface of the sample. The reflection of the light allows an accurate measurement of the distance between probe and sample surface (Fig. 2). The acquisition was performed with a frequency of 100 Hz and the mean of ten measured values was taken.

The ribblets were placed underneath the probe approximately 10 s after the ejection and the change in the ribblet thickness was monitored for 30 min, whereby the distance between the ribblet surface and the measurement head decreases with increasing elastic recovery of the ribblet. Using Eq. (3), the out-of-die elastic recovery can be calculated. It is composed of the in-die elastic recovery and the elastic recovery which takes place after ejection and is measured with the chromatic confocal probe.

$$ER_{out-of-die(x)} = \frac{(h_{con(x)} - h_{min})}{h_{min}} \times 100 \tag{3}$$

where h_{con} is the height of the ribblet at a timepoint x and h_{min} the minimum thickness between upper and lower punch during compression.

2.6.2. Long term measurement of elastic recovery

To evaluate when the elastic recovery is completed, the height of ten ribblets per compression pressure setting was measured with a digital calliper (Mitutoyo) at different time points (0 min, 30 min, 60 min, 120 min, 180 min and daily for 9 further days). To test whether a considerably elastic recovery occurs as well in the radial direction, the length and width of ten ribblets per compression pressure where measured directly after ejection and after seven days. The dimensions were
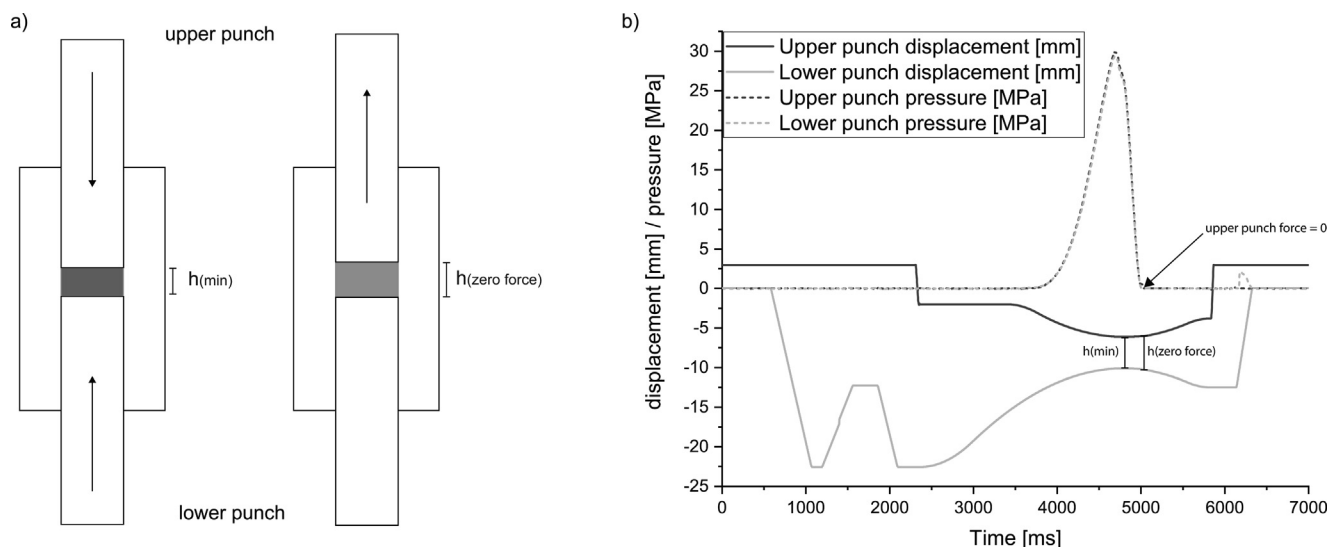
Fig. 1. Principle of in-die elastic recovery measurement; a) minimum distance and distance at zero upper punch force for the in-die elastic recovery calculation; b) upper and lower punch displacement and pressure during a compression cycle of MCC mimicking 60% solid fraction and 4 mm gap width.
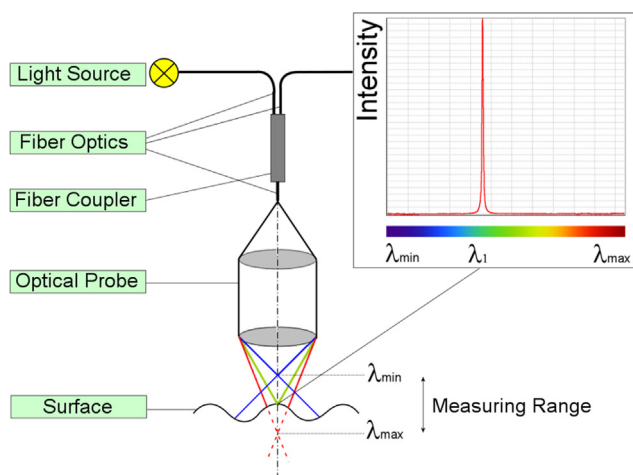

Fig. 2. Measurement principle for ribblet thickness by chromatic confocal distance measurement (by courtesy of Precitec Optronik GmbH, Germany).

measured in triplicate and the mean was taken. The total elastic recovery in axial direction was calculated by Eq. (4),

$$ER_{total} = \frac{(h_t - h_{min})}{h_{min}} \times 100 \qquad (4)$$

where h_t is the height at a certain time point t and h_{min} the minimum distance between upper and lower punch under load.

$$ER_{length} = \frac{(l_t - l_{die})}{l_{die}} \times 100$$

$$ER_{width} = \frac{(w_t - w_{die})}{w_{die}} \times 100 \qquad (5)$$

The elastic recovery in radial direction is divided into the elastic recovery of the length (ER_{length}) and the elastic recovery of the width (ER_{width}) of the compact. They can be calculated according to Eq. (5), where l_t and w_t are the length and the width of the ribblet at a timepoint t and l_{die} and w_{die} the length and the width of the rectangular punch.

2.7. Solid fraction prediction/learning phase

To overcome the limitations of the original approach (Reimer and Kleinebudde, 2019), the slow out-of-die elastic recovery should be implemented into the model. A flow-chart (Fig. 3) illustrates the

simulation/mimicking process with the additional learning step. The learning steps are performed as described in Section 2.4 at the maximum force of 51 kN (255 MPa) at three different filling heights. Additionally, the height of the test ribblets was measured after one minute with a digital calliper (Mitutoyo). The desired settings or properties – RS, GW, SF – were defined and the resulting SCF (shown in MPa for the Styl'One and in kN/cm for the roll compactor) was determined according to the method introduced by Reimer and Kleinebudde (2019). Then, an additional learning phase was added to consider the out-of-die elastic recovery and its pressure dependence. A pressure-density curve was recorded producing one ribblet at the adapted filling depth and compaction pressure. This compaction pressure included a safety margin of 20% to ensure that the target pressure is within the investigated pressure range because the pressure density curve cannot be extrapolated to higher pressures. The height of the learning ribblet is measured one minute after ejection. This time can be prolonged e.g. for materials showing a considerably slow elastic recovery.

2.8. Mimicking of an API containing formulation

An ibuprofen containing powder blend should be compacted on a Gerteis Mini-Pactor. To save material and time in process development, the process should be mimicked using the above mentioned method (Section 2.7). The roll compaction process was simulated on the Styl'One Evolution at a GW of 3 mm and a RS of 2 rpm in order to find the appropriate SCF to obtain ribblets with a SF of 80%. The predicted SCF was transferred to the roll compaction process and ribbons were produced. The ribbons and ribblets were characterized regarding their SF (according to Section 2.9.1) to determine the prediction accuracy.

2.9. Characterisation of ribbons and ribblets

2.9.1. Powder pycnometry

The powder pycnometer GeoPyc 1360 (Micromeritics) was used to determine the envelope density of ribbons and ribblets (Zinchuk et al., 2004). The ribbon samples were sieved with a 2000 μm sieve to remove fines. The ribblets were cleaned from dust before the measurements. The measurement chamber with a diameter of 25.4 mm was used and the default conversion factor of 0.5153 cm³/mm was set. The sample volume was kept constant at approximately 15% of the chamber volume. Three blank cycles to determine the volume of the Dry Flo powder and three measurement cycles to determine the sample volume were performed with a consolidation force of 51 N. The relative density
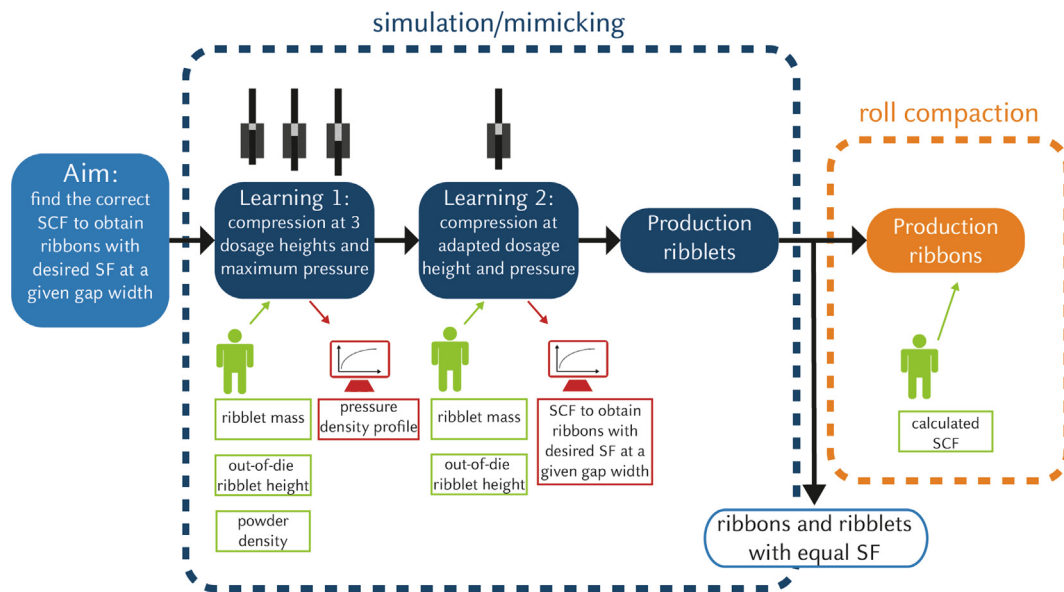
Fig. 3. Flow-chart of the simulation/mimicking process to determine the SCF needed to obtain ribbons with the desired SF at a given gap width.

$\rho_{compact}$ or solid fraction *SF* of the compact can be calculated by using Eq. (6) where $\rho_{envelope}$ is the envelope density of the compact – composed of the mass *m* and the envelope volume *V* - and ρ_{powder} is the powder true density of the starting material. The measurements were performed in triplicate and the mean was calculated.

$$SF_{compact} = \frac{\rho_{envelope}}{\rho_{powder}} \times 100 = \frac{\frac{m}{V}}{\rho_{powder}} \times 100 \qquad (6)$$

2.9.2. Chromatic confocal measurements

For the SF determination in the chromatic confocal measurement part, the length and the width of the ribblets were assumed to be constant, 20 and 10 mm respectively. The change in ribblet height was detected by the sensor. Thus, the ribblet volume can be calculated. Knowing the mass, which was determined by an analytical balance, and the powder true density, the solid fraction can be calculated for each time point *t* according to Eq. (6).

2.9.3. Measurement with calliper

Due to the very regular shape of the ribblets, their volume can also be measured by using a calliper. The width, length and height were determined two days after production. The volume was calculated, and the weight was determined with an analytical balance. The solid fraction could then be calculated according to Eq. (6).

2.10. Error in solid fraction prediction

Two types of SF prediction errors are used in this publication. First, the error between the desired ribblet SF and the measured ribblet SF after elastic recovery which is calculated following Eq. (7).

$$error_{ribblet} = \frac{|SF_t - SF_{ribblet}|}{SF_t} \times 100 \qquad (7)$$

where SF_t is the target solid fraction and $SF_{ribblet}$ the measured ribblet solid fraction.

Second, the error between the target ribbon SF compared to the measured ribbon SF. It is calculated according to Eq. (8).

$$error_{ribbon} = \frac{|SF_t - SF_{ribbon}|}{SF_t} \times 100 \qquad (8)$$

where SF_t is the target solid fraction and SF_{ribbon} the measured ribbon solid fraction.

3. Results and discussion

3.1. Connection between solid fraction, compression pressure, specific compaction force, gap width, dosage height and feed screw speed

To understand better the connection between the SCF on a roll compactor and the compression pressure on the uniaxial compaction simulator, roll compaction of MCC, lactose and DCPA was simulated on the Styl'One at a constant RS of 2 rpm, at several SCFs and at GWs of 2 and 4 mm (Reimer and Kleinebudde, 2018).

The ribblet SF is strongly influenced by the applied SCF and the GW (Fig. 4b). This influence is material dependent due to their different compressibility and compaction behaviour. A relatively small change in SCF leads to a higher change in SF for MCC than for lactose or DCPA. The total SFs of DCPA are smaller than for MCC and lactose at the same SCF due to its poor compressibility. The bigger the GW the smaller is the resulting solid fraction applying the same SCF.

Linear relationships between compression pressure and simulated SCF were found for the three investigated materials. Interestingly, a certain SCF does not correspond to one single compression pressure but differs between the tested substances (Fig. 4a). This difference could be explained, amongst other factors, by varying nip angles of the materials together with the varying extent of elastic recovery after compaction that results in different times and distances where pressure is exerted on the powders by the punches.

The GW has a distinct influence on the compression pressure (Fig. 4a). A given compression pressure results in a lower SCF for a low GW compared to a high GW. The increase in dosage height on the compaction simulator with increasing SCF and GW can be transferred to the increase in the feed screw speed in roll compaction, exemplarily shown for DCPA and MCC in Fig. 5. In both cases, a higher mass of powder is required to fill the constant volume under pressure (GW or minimum height), if the SF is higher. The curves are steeper for MCC since the change in SF in the investigated range of SCF is higher.

3.2. Prediction of solid fraction with the minimum height method

Hybrid modeling of the roll compaction process leads to compacts showing the same SF as ribbons. Nevertheless, the predictive ability of the method shows a lack of accuracy (Reimer and Kleinebudde, 2019). The predicted SFs and the ones measured after elastic recovery for MCC and lactose ribblets are compared in Fig. 6. A systematic over-
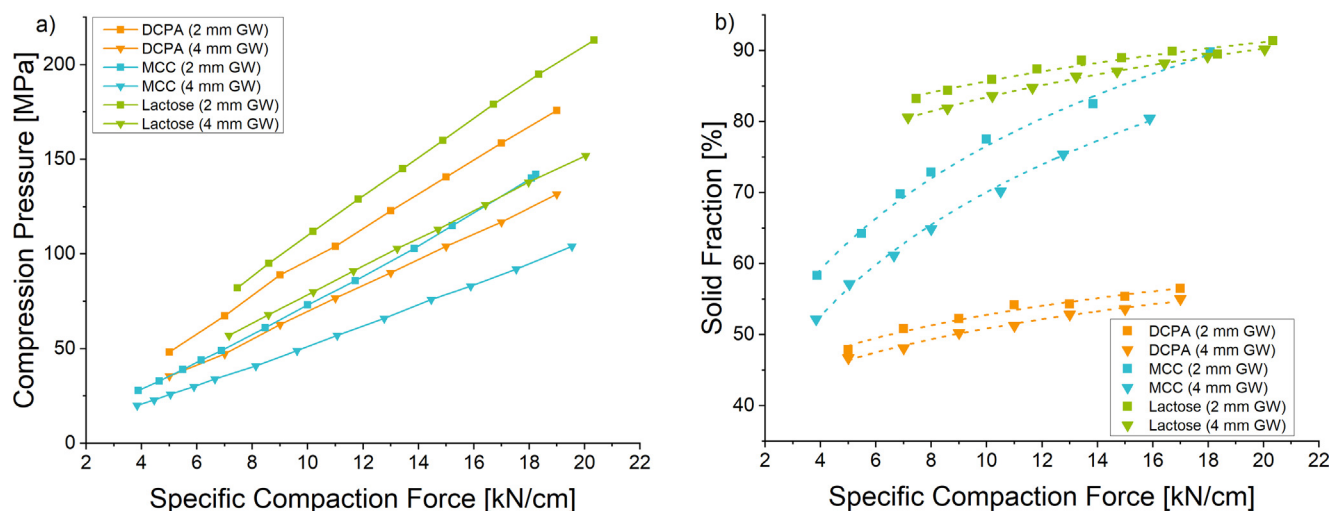
Fig. 4. Correlation between simulated specific compaction force and a) compression pressure and b) measured solid fraction for DCPA, MCC and lactose ribblets.

estimation of the SF by the minimum height method can be seen for both materials. It should be emphasized that the error of prediction for MCC is more pronounced than for lactose. These results are in accordance with findings from Wunsch et al. (2019) where in-die and out-of-die compressibility of lactose, MCC and DCPA are compared. In-die compressibility curves lead to smaller porosity values/higher SFs than the out-of-die analysis.

The reason for the observed over-estimation lays in the learning phase (described in Section 2.4). Two main weaknesses explain the lack in prediction accuracy of the minimum height method. First, the minimum distance between the punches does not represent the final thickness of the compact after ejection because it does not consider the elastic recovery of the compacts. Second, the automatic learning phase is performed at a default force of 51 kN (255 MPa) and not at the finally used one so that the pressure dependency of the elastic recovery cannot be considered.

3.3. In-die elastic recovery

3.3.1. Material, pressure and gap width dependence of in-die elastic recovery

The elastic recovery of a compact can be divided into a fast recovery, which already takes place in the die during the decompression phase, and a slow one, which takes place after ejection of the compact.

In a first step, the fast in-die elastic recovery should be implemented to the simulation to improve the predictive accuracy for the SF.

The in-die elastic recovery of MCC, HPMC, Carrageenan, lactose and DCPA ribblets was measured at varying GWs and SCFs. The results are shown in Fig. 7. To allow a better comparability between the different materials, the simulated SCF is displayed in the corresponding compression pressure in MPa.

Carrageenan shows with 5.0–8.3% the highest in-die elastic recovery, followed by HPMC (4.4–5.4%) and MCC (2.2–3.8%). DCPA and lactose undergo a smaller in-die elastic recovery of 1.1–2.2% and 0.7–1.6%, respectively. The in-die elastic recovery is dependent on the applied compression pressure. At low pressure, the two celluloses HPMC and MCC as well as Carrageenan show a decrease in in-die elastic recovery with an increasing compression pressure. At higher pressures, the in-die elastic recovery of MCC and HPMC (Fig. 7a, b) increases again, what is in accordance with literature (Mazel et al., 2013). Antikainen and Yliruusi (2003) stated that the decrease in elastic recovery at low pressures followed by the increase at high pressures relates to trapped air inside the powder bed. For the predominantly brittle deforming materials lactose and DCPA (Fig. 7d, e), an increase in compression pressure leads to an increase of the in-die elastic recovery that was observed as well by Antikainen and Yliruusi (2003).

An increased simulated GW leads to a higher in-die elastic recovery for all tested materials. In case of a higher simulated GW, the dosage
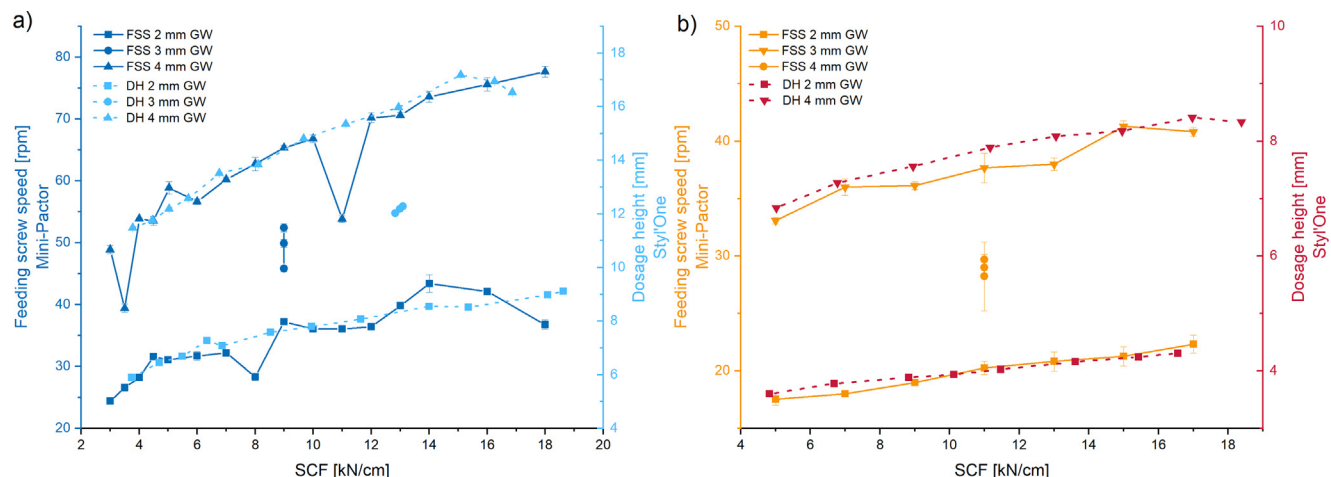

Fig. 5. Comparison of the correlation between feeding screw speed (FSS) and SCF on the Mini-Pactor (mean over one minute process time) and dosage height (DH) on the Styl'One at different gap widths (GW) for a) MCC and b) DCPA; n = 30, mean ± SD.

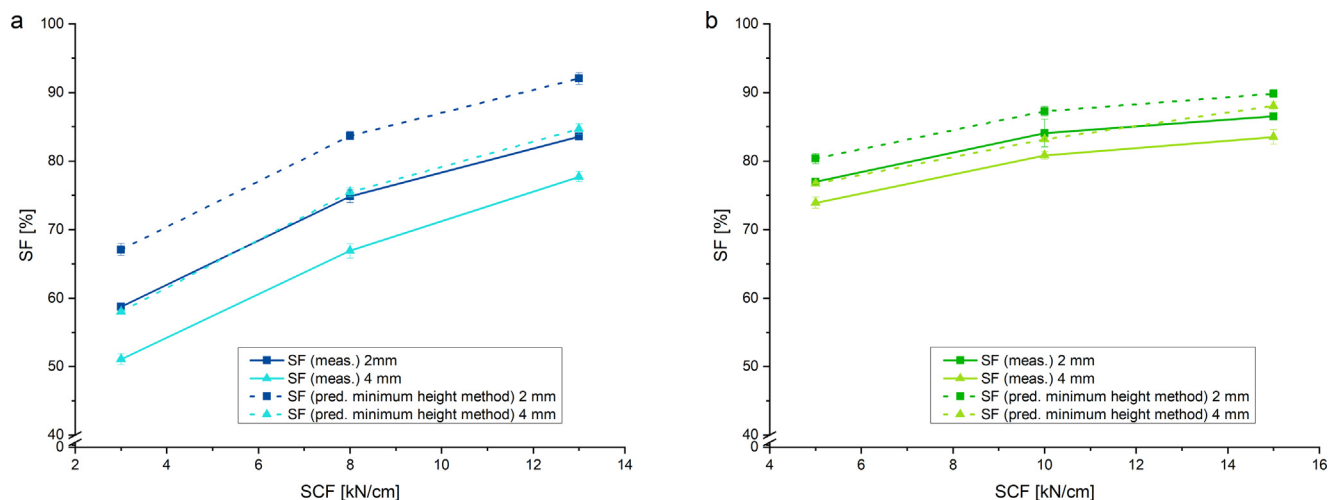**Fig. 6.** Comparison between the measured ribblet solid fraction and the predicted by the minimum height method for a) MCC and b) lactose; n ≥ 3, mean ± SD.

height is increased and a bigger amount of powder is compressed with the same compaction pressure. The material undergoes less plastic deformation, but more elastic deformation and the stored elastic energy can be released more easily after compaction in form of elastic recovery.

3.3.2. In-die elastic recovery of MCC in dependence on dwell time and mimicked roll speeds

The in-die elastic recovery of MCC decreases with an increasing dwell time from 1.4% at 600 ms to 0.8% at 3000 ms (Fig. 8a). An increase in dwell time leads to a more pronounced plastic deformation and thus to less relaxation (Anuar and Briscoe, 2009).

The influence of the RS on the in-die elastic recovery was tested by mimicking RSs between 3 and 11 rpm. No relevant change could be observed, the values fluctuated around 3.5% (Fig. 8b). From Anuar and

Briscoe (2009) it is known that starch tablets show a compression velocity dependent elastic recovery. However, it was stated as well that the speed of industrial rotary die tablet presses is too high to observe this phenomenon in practice. The same can be assumed for the mimicked RSs that are too high to observe a reduction in elastic recovery of the MCC compacts with a decreasing velocity. Furthermore, MCC shows a smaller extent of time dependent plastic deformation than starch (David and Augsburger, 1977).

3.3.3. Solid fraction prediction with the zero-force method

To implement the findings about the in-die elastic recovery into the hybrid modeling approach, the original minimum distance method was adapted. By determining the in-die elastic recovery (Section 2.5), the calculation of the ribblet solid fraction can be modified. Instead of using the minimum distance between upper and lower punch, the distance is
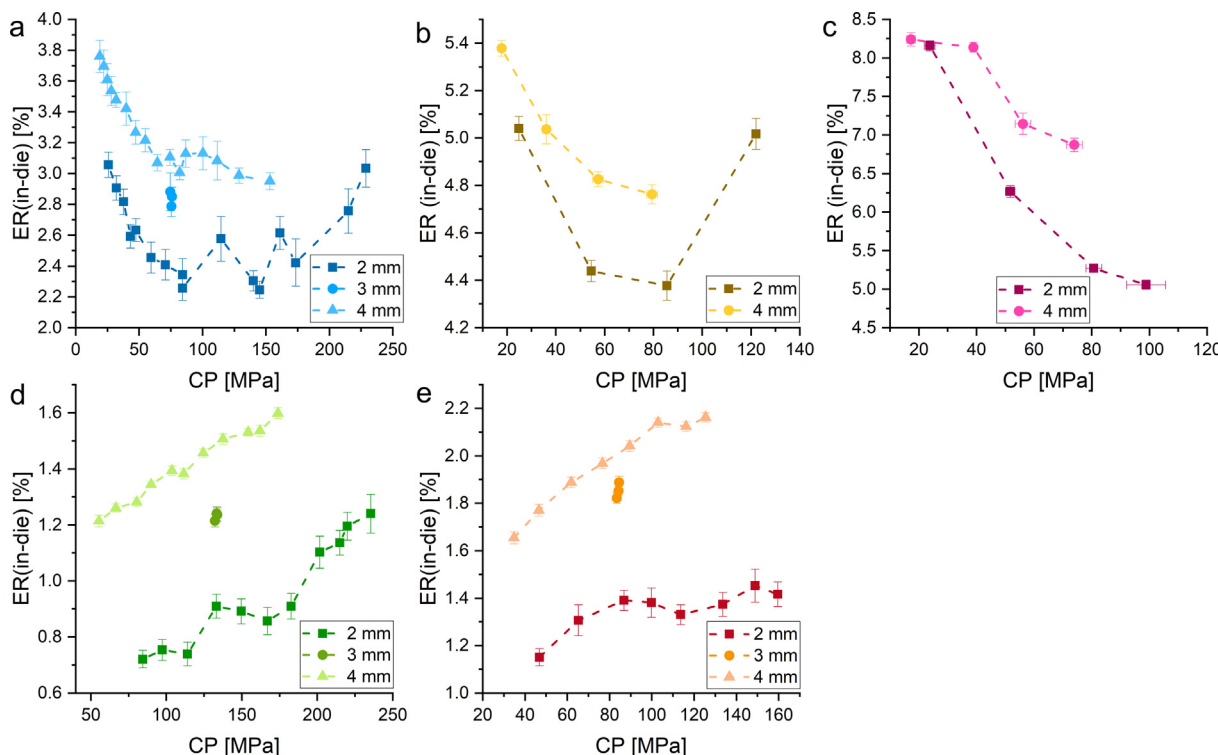

Fig. 7. In-die elastic recovery in correlation with the compression pressure at different gap widths for a) MCC, b) HPMC, c) carrageenan, d) lactose, e) DCPA; n ≥ 20, mean ± SD.
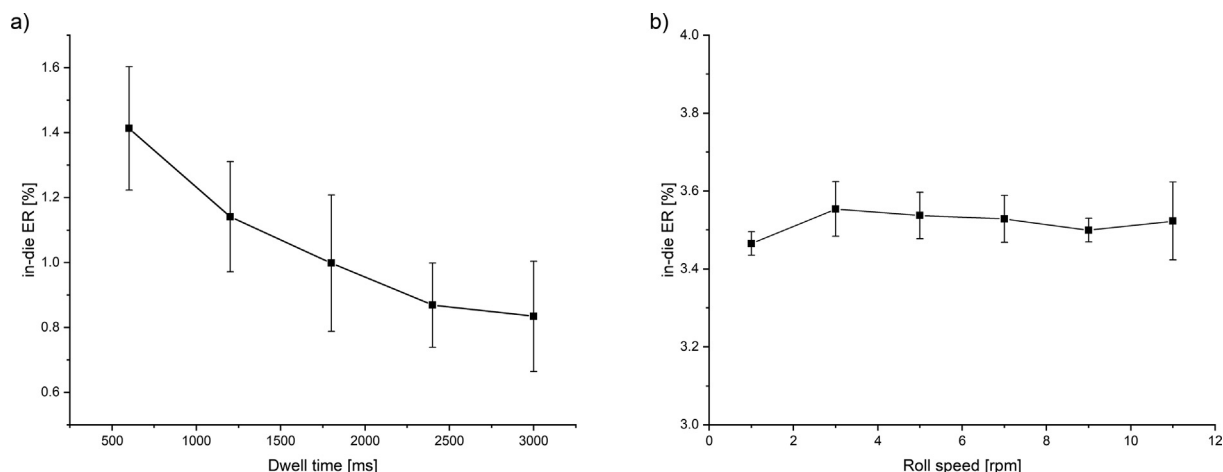
Fig. 8. In-die elastic recovery of MCC compacts in dependence on the a: dwell time and b: roll speed; n = 10, mean ± SD.

taken when the force at the upper punch falls to zero during its upward movement after the compression.

Fig. 9 shows the measured ribblet solid fraction compared to the values which were predicted with the zero force method. For MCC (Fig. 9a), a clear reduction in the prediction errors can be observed. Nevertheless, the predicted SF are still over-estimated compared to the measured solid fraction. This difference can be explained by the fact that the elastic recovery is not completed inside the die but continues after ejection.

Fig. 9b shows on the other hand the accurate solid fraction prediction for the lactose compacts which is considerably better compared to the predictions for MCC. This leads to the question how the two materials differ in terms of their slow out-of-die elastic recovery.

3.4. Out-of-die elastic recovery

The slow elastic recovery, which occurs after ejection, was investigated with MCC, lactose and carrageenan compacts. The gain in height was monitored contactless with a chromatic confocal probe for 30 min (Section 2.6.1). The results are depicted in Fig. 10.

Carrageenan shows the largest elastic recovery after ejection (17–22%), followed by MCC (7–10%) and lactose (3–5%). For lactose compacts, the elastic recovery is comparatively small and seems already to be completed only seconds after the ejection. The compacts containing of lactose showed capping at the edges what is in accordance with the findings of Maarschalk et al. (1997). They stated as well that plastic materials like MCC can release the stored energy in volume extension whereas the stress release in compacts containing brittle

materials like lactose leads to capping issues because they are not able to undergo enough elastic recovery.

The extent of the out-of-die elastic recovery is dependent on the applied compression pressure. However, there is no linear relationship between pressure and the elastic recovery after 30 min (Fig. 10c,f,i). The elastic recovery of MCC compacts decreases at compression pressures between 50 and 150 MPa before it increases again at 200 MPa what is in accordance with the observed in-die effects (Section 3.3). The elastic recovery of Carrageenan compacts decreases as well at low pressures and increases between 150 MPa and 250 MPa. The elastic recovery of lactose compacts fluctuates between 3 and 5% in the considered pressure range showing no clear trend.

The change in solid fraction due to the elastic recovery is most pronounced in the first seconds because the speed of relaxation is highest at the beginning and decreases with the time. Carrageenan shows the highest decrease in solid fraction of up to 15% due to volume increase. The solid fraction of MCC compacts decreases by around 5% whereas the solid fraction of lactose decreases by less than 2.5%.

3.5. Long-term total elastic recovery

The two extreme materials carrageenan and lactose were chosen to monitor the elastic recovery in long-term. The thickness of the ribblets produced at 50, 150 and 250 MPa was measured with a calliper at different time points over a period of 10 days. The results are shown in Fig. 11.

As seen in the chromatic confocal measurements, the elastic recovery of carrageenan (16–25%) is much more pronounced compared
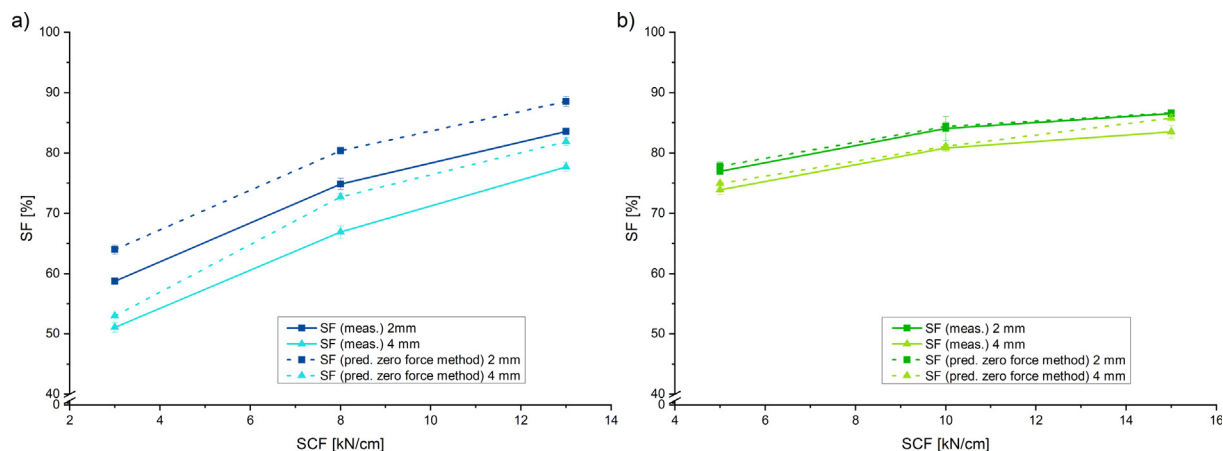

Fig. 9. Comparison between the measured ribblet SF and the predicted by the zero force method for a) MCC and b) lactose; n ≥ 3; mean ± SD.
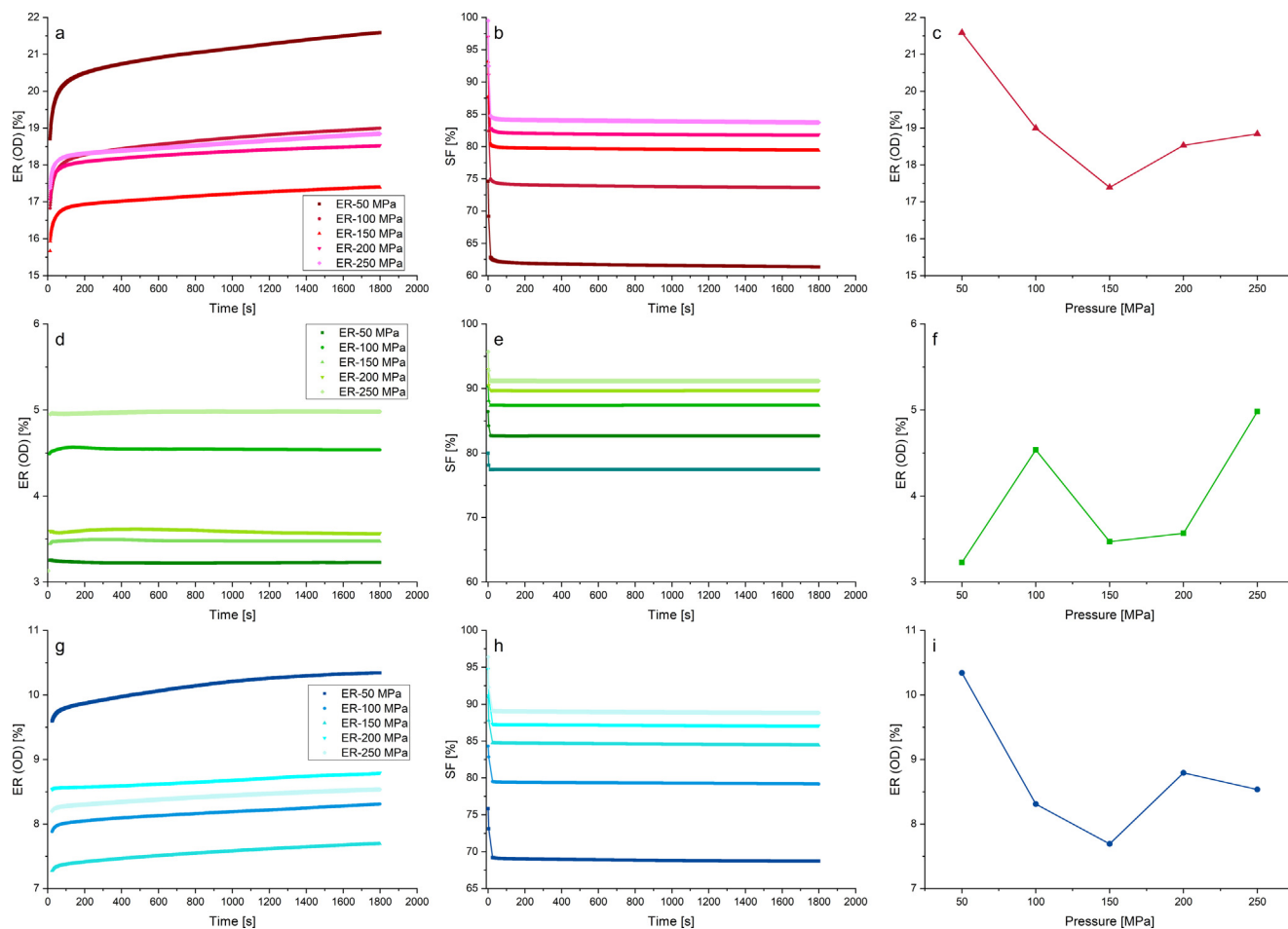
Fig. 10. Out of die axial elastic recovery (ER(OD)) measured by chromatic confocal sensor, solid fraction (SF) and out-of-die elastic recovery after 30 min for carrageenan (a-c), lactose (d-f) and MCC (g-i); n = 2, mean.

to lactose (3–5.5%). The total elastic recovery increases with an increasing compression pressure for lactose, whereas it decreases for carrageenan. The fluctuations for the total elastic recovery of lactose ribblets at 250 MPa may be due to non-visible cracks in the inside of the compacts or to person related measurement errors. The increase in height of carrageenan compacts continues over six days whereas the lactose compacts show no relevant difference in height after the first minutes. In roll compaction, not the pure excipients but mixtures are

used so that it can be expected that the elastic recovery will be lower compared to the extreme example carrageenan.

3.6. Elastic recovery in radial direction

The elastic recovery in radial direction was monitored as well over a period of one week. The results are shown in Fig. 12.

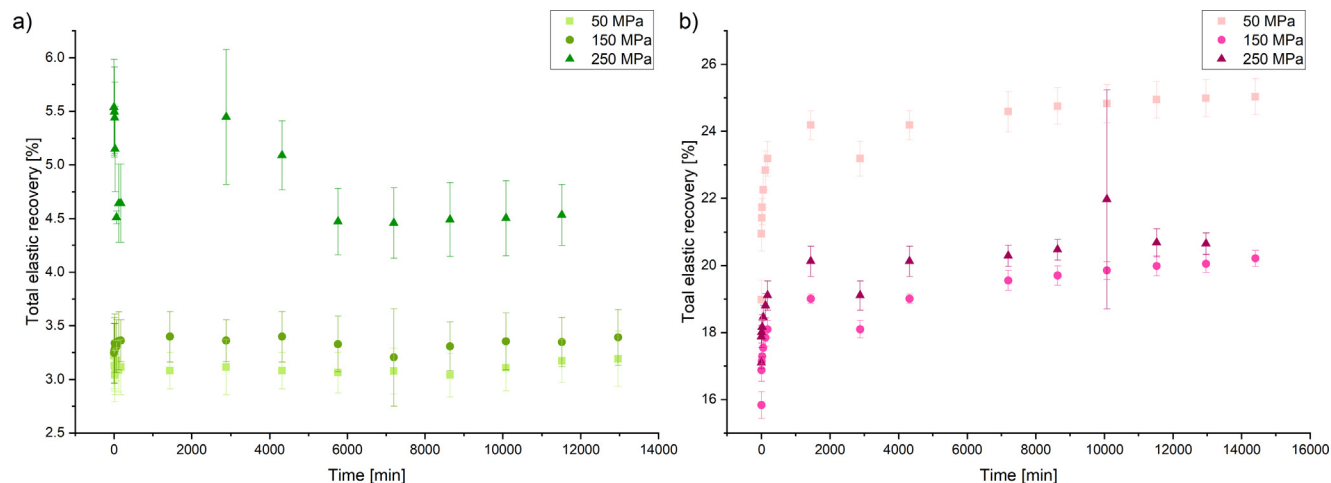The elastic recovery in radial direction is 6 to 20 times less

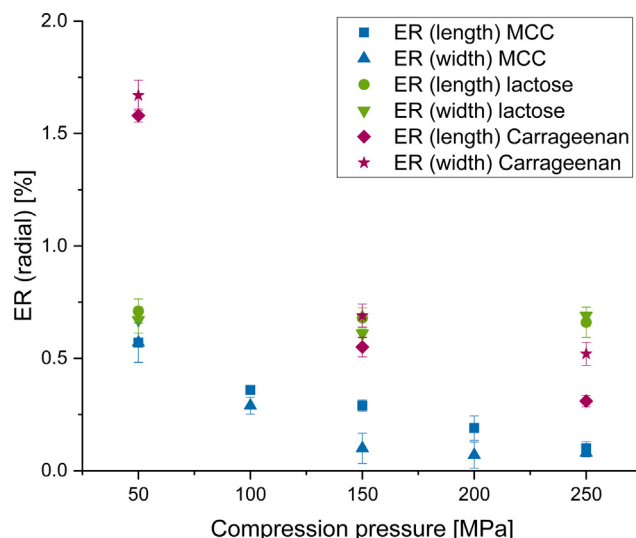**Fig. 11.** Long-term total elastic recovery of a) lactose and b) carrageenan ribblets; n = 10, mean ± SD.

Fig. 12. Elastic recovery in radial direction depending on the compression pressure for MCC, lactose and carrageenan; n = 10, mean ± SD.

Table 3
Solid fraction prediction for MCC ribblets with additional learning phase.

Gap width [mm]	SCF (n = 25) [kN/cm]	Predicted ribblet solid fraction (n = 1) [%]	Measured ribblet solid fraction (n = 25) [%]	Error$_{ribblet}$ [%]
2	4.3	60	61.0	1.7
4	5.8	60	59.8	0.3
2	12.9	80	80.4	0.5
4	20.0	80	81.3	1.6

well for the elastic recovery outside of the die (elastic recovery method), considerably higher prediction precision of the solid fraction could be achieved and the errors$_{ribblet}$ could be reduced to values below 2.5%.

3.8. Mimicking of roll compaction process with an ibuprofen containing formulation

The hybrid modeling approach was so far only tested with pure excipients. To show that the approach is also applicable to more complex systems, an ibuprofen containing formulation was mimicked (Berkenkemper, 2019). The aim was to find the appropriate SCF to obtain ribbons with a solid fraction of 80% at a GW of 3 mm and at a RS of 2 rpm.

The predicted SCF to obtain ribbons with a solid fraction of 80% was found to be 8.48 kN/cm. The solid fraction of the ribblets was measured with the powder pycnometer after two days of storage to confirm the prediction. The ribblets had a solid fraction of 78.9% ± 0.8% what corresponds to a prediction error of 1.4%. The error$_{ribblet}$ lays within the range of the tested pure MCC (Section 3.7).

Roll compaction was performed with the Gerteis Mini-Pactor following the predicted setting of 8.5 kN/cm. The ribbon solid fraction measured two days after production with the powder pycnometer was 81.8% ± 0.5%. This results in an error$_{ribbon}$ of 2.3% in relation to the target solid fraction of 80%.

This prediction error is only slightly higher than the measurement inaccuracies of the powder pycnometry what underlines the high precision of the method compared to the methods known from literature. Thus, hybrid modeling of roll compaction is not only applicable to pure materials but as well on formulations containing an API and different excipients.

For the mimicking of the roll compaction process and the prediction of the correct process parameters only a small amount of material is necessary. When the feed shoe is used, an amount of ~150 g powder-blend is needed to assure an accurate filling of the die. This is comparable to the value reported by Nesarikar et al. (2012a,b). When the die is filled by hand, a limited amount of only ~5 g is sufficient, which is a great advantage of the hybrid modeling approach.

pronounced than in the axial direction which confirms findings from literature (Picker, 2001). This is because the compaction pressure during tableting is applied in axial direction onto the powder bed. Moreover, the elastic expansion in radial direction can only take place after the compact has been ejected (Train, 1956; Haware et al., 2010).

The elastic recovery in width and length is smaller than 0.8% except for carrageenan which shows an elastic recovery of 1.6% at 50 MPa compression pressure. For MCC and carrageenan, the radial elastic recovery decreases with an increase in compression pressure. The radial elastic recovery of lactose compacts ranges around 0.7% for the three tested compression pressures. Hence, the radial elastic recovery has no relevant impact on the change in SF compared to the axial elastic recovery.

3.7. Prediction of solid fraction with additional learning phase

As shown in the previous sections, the biggest part of the axial elastic recovery is completed within a few seconds to minutes after ejection for most of the studied materials so that the SF will not change considerably afterwards. It was shown as well that the elastic recovery in radial direction is smaller than 1.6% for the tested materials and can be neglected in the calculations of the SF.

Based on these findings, an additional learning step was implemented in the software to better target the SF. To consider the non-linear pressure dependency of the elastic recovery, the learning is performed not at 51 kN (255 MPa) as it was done in the automatic learning phase but at the finally desired compression pressure (Section 2.7). The height of the compact is measured with a calliper one minute after ejection. The time until the height measurement is performed can be adapted individually depending on the properties of the used materials. The height of the compact is then used to calculate the out-of-die volume of the compact together with the dimensions of the rectangular punch (10 × 20 mm). This additional learning phase was tested with MCC. The aim was to determine the SCF to produce ribblets with solid fractions of 60 and 80% at GWs of 2 and 4 mm and a RS of 2 rpm. The solid fraction was measured according to 2.9.3. The results are shown in Table 3. The prediction errors$_{ribblet}$, which were calculated by Eq. (7), range between 0.3 and 1.7%.

Comparing the different methods of solid fraction calculation (Fig. 13), it can be seen that the new learning phase leads to a significant improvement in prediction accuracy. The first step was to consider the in-die elastic recovery (zero force method), what leads to a decrease of the prediction errors$_{ribblet}$ from 13 to 7%. By accounting as

4. Conclusion

The pressure dependent elastic recovery of ribblets – in-die and out-of-die – could be implemented successfully to the model. This allowed to overcome the weaknesses regarding the prediction accuracy of the original model. The relation between the SCF and the ribbon SF on a roll compactor can be given accurately for materials with different deformation behaviours. The hybrid modeling approach can simulate and mimic the roll compaction process correctly, to find the appropriate settings for the process and finally, to produce ribbons with the desired solid fraction with only small experimental effort and material consumption (~5 g). The prediction errors for the solid fraction were reduced considerably to values below 2.3% for the roll compaction simulation of pure MCC as well as for an API containing formulation.
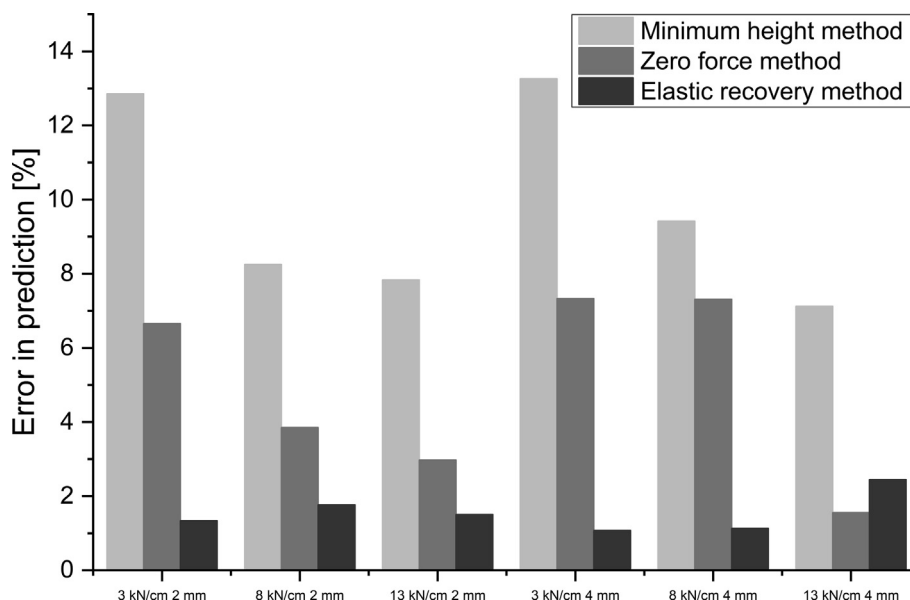
Fig. 13. Prediction errors as indicator for the quality of the prediction of the solid fraction of MCC ribblets at varying SCFs and GWs shown for three methods considering either the ribblet thickness at maximum pressure, the in-die elastic recovery thickness or the out-of-die elastic recovery thickness.

Declaration of Competing Interest

The authors declare the following financial interests/personal relationships which may be considered as potential competing interests.

Acknowledgements

References

Akseli, I., Ladyzhynsky, N., Katz, J., He, X.R., 2013. Development of predictive tools to assess capping tendency of tablet formulations. Powder Technol. 236, 139–148. https://doi.org/10.1016/j.powtec.2012.04.026.

Antikainen, O., Yliruusi, J., 2003. Determining the compression behaviour of pharmaceutical powders from the force-distance compression profile. Int. J. Pharm. 252 (1–2), 253–261. https://doi.org/10.1016/S0378-5173(02)00665-8.

Anuar, M.S., Briscoe, B.J., 2009. The elastic relaxation of starch tablets during ejection. Powder Technol. 195 (2), 96–104. https://doi.org/10.1016/j.powtec.2009.05.019.

Armstrong, N.A., Haines-Nutt, R.F., 1972. Elastic recovery and surface-area changes in compacted powder systems. J Pharm and Pharmacol 24, 135.

Berkenkemper, S., 2019. Funktionalität von Zerfallsbeschleunigern mit unterschiedlichen Mechanismen nach Walzenkompaktierung, Diploma thesis, Martin-Luther-University Halle-Wittenberg, 2019.

Bi, M.D., Alvarez-Nunez, F., Alvarez, F., 2014. Evaluating and modifying Johanson's rolling model to improve its predictability. J. Pharm. Sci. 103, 2062–2071. https://doi.org/10.1002/jps.24012.

Cunningham, 2005. Experimental Studies and Modeling of the Roller Compaction of Pharmaceutical Powders (Doctoral Thesis).

David, S.T., Augsburger, L.L., 1977. Plastic-flow during compression of directly compressible fillers and its effect on tablet strength. J. Pharm. Sci. 66, 155–159. https://doi.org/10.1002/jps.2600660205.

Dec, R.T., Zavaliangos, A., Cunningham, J.C., 2003. Comparison of various modeling methods for analysis of powder compaction in roller press. Powder Technol. 130, 265–271. https://doi.org/10.1016/s0032-5910(02)00203-6.

Guigon, P., Simon, O., 2003. Roll press design—influence of force feed systems on compaction. Powder Technol. 130, 41–48. https://doi.org/10.1016/s0032-5910(02)00223-1.

Haware, R.V., Tho, I., Bauer-Brandl, A., 2010. Evaluation of a rapid approximation method for the elastic recovery of tablets. Powder Technol. 202 (1–3), 71–77. https://doi.org/10.1016/j.powtec.2010.04.012.

Ilic, I., Govedarica, B., Sibanc, R., Dreu, R., Srcic, S., 2013. Deformation properties of pharmaceutical excipients determined using an in-die and out-die method. Int. J. Pharm. 446, 6–15. https://doi.org/10.1016/j.ijpharm.2013.02.001.

Johanson, J.R., 1965. A rolling theory for granular solids. J. Appl. Mech. 32 (4), 842–848. https://doi.org/10.1115/1.3627325.

Katz, J.M., Roopwani, R., Buckner, I.S., 2013. A material-sparing method for assessment of powder deformation characteristics using data collected during a single compression–decompression cycle. J. Pharm. Sci. 102 (10), 3687–3693. https://doi.org/10.1002/jps.23676.

Leane, M., Pitt, K., Reynolds, G., Workin, M.C.S.M., 2015. A proposal for a drug product Manufacturing Classification System (MCS) for oral solid dosage forms. Pharm. Dev. Technol. 20, 12–21. https://doi.org/10.3109/10837450.2014.954728.

Maarschalk, K.V.D.V., Zuurman, K., Vromans, H., Bolhuis, G.K., Lerk, C.F., 1997. Stress relaxation of compacts produced from viscoelastic materials. Int. J. Pharm. 151 (1), 27–34.

Mahmah, O., Adams, M.J., Omar, C.S., Gururajan, B., Salman, A.D., 2019. Roller compaction: Ribbon splitting and sticking. Int. J. Pharm. 559, 156–172. https://doi.org/10.1016/j.ijpharm.2019.01.031.

Mazel, V., Busignies, V., Diarra, H., Tchoreloff, P., 2013. On the links between elastic constants and effective elastic behavior of pharmaceutical compacts: Importance of poisson's ratio and use of bulk modulus. J. Pharm. Sci. 102 (11), 4009–4014. https://doi.org/10.1002/jps.23710.

Michrafy, A., Diarra, H., Dodds, J.A., Michrafy, M., Penazzi, L., 2011. Analysis of strain stress state in roller compaction process. Powder Technol. 208, 417–422. https://doi.org/10.1016/j.powtec.2010.08.037.

Muliadi, A.R., Litster, J.D., Wassgren, C.R., 2012. Modeling the powder roll compaction process: Comparison of 2-D finite element method and the rolling theory for granular solids (Johanson's model). Powder Technol. 221, 90–100. https://doi.org/10.1016/j.powtec.2011.12.001.

Nesarikar, V.V., Vatsaraj, N., Patel, C., Early, W., Pandey, P., Sprockel, O., Gao, Z., Jerzewski, R., Miller, R., Levin, M., 2012a. Instrumented roll technology for the design space development of roller compaction process. Int. J. Pharm. 426, 116–131. https://doi.org/10.1016/j.ijpharm.2012.01.032.

Nesarikar, V.V., Patel, C., Early, W., Vatsaraj, N., Sprockel, O., Jerzweski, R., 2012b. Roller compaction process development and scale up using Johanson model calibrated with instrumented roll data. Int. J. Pharm. 436, 486–507. https://doi.org/10.1016/j.ijpharm.2012.06.027.

Nkansah, P., Wu, S.J., Sobotka, S., Yamamoto, K., Shao, Z.J., 2008. A novel method for estimating solid fraction of roller-compacted ribbons. Drug Dev. Ind. Pharm. 34, 142–148. https://doi.org/10.1080/03639040701484387.

Paronen, P., Juslin, M., 1983. Compressional characteristics of 4 starches. J. Pharm. Pharmacol. 35, 627–635. https://doi.org/10.1111/j.2042-7158.1983.tb02855.x.

Patel, B.A., Adams, M.J., Turnbull, N., Bentham, A.C., Wu, C.Y., 2010. Predicting the pressure distribution during roll compaction from uniaxial compaction measurements. Chem. Eng. J. 164 (2–3), 410–417. https://doi.org/10.1016/j.cej.2009.12.022.

Peter, S., Lammens, R.F., Steffens, K.-J., 2010. Roller compaction/dry granulation: Use of the thin layer model for predicting densities and forces during roller compaction. Powder Technol. 199 (2), 165–175. https://doi.org/10.1016/j.powtec.2010.01.002.

Picker, K.M., 2001. Time dependence of elastic recovery for characterization of tableting materials. Pharm. Dev. Technol. 6 (1), 61–70. https://doi.org/10.1081/PDT-100000014.

Reimer, H.L., Kleinebudde, P., 2019. Hybrid modeling of roll compaction processes with the styl'one evolution. Powder Technol. 341, 66–74. https://doi.org/10.1016/j.

powtec.2018.02.052.

Reimer, H.L., Kleinebudde, P., 2018. Roll compaction simulation - connection between specific compaction force, compression pressure and gap width. 8th Compaction Simulation Forum Europe, Cambridge.

Reynolds, G., Ingale, R., Roberts, R., Kothari, S., Gururajan, B., 2010. Practical application of roller compaction process modeling. Comput. Chem. Eng. 34 (7), 1049–1057. https://doi.org/10.1016/j.compchemeng.2010.03.004.

Roberts, R.J., Rowe, R.C., 1987. The compaction of pharmaceutical and other model materials - a pragmatic approach. Chem. Eng. Sci. 42, 903–911. https://doi.org/10.1016/0009-2509(87)80048-9.

Sun, C.C., Kleinebudde, P., 2016. Mini review: Mechanisms to the loss of tabletability by dry granulation. Eur. J. Pharm. Biopharm. 106, 9–14. https://doi.org/10.1016/j.ejpb.2016.04.003.

Toson, P., Lopes, D.G., Paus, R., Kumar, A., Geens, J., Stibale, S., Quodbach, J., Kleinebudde, P., Hsiao, W.-K., Khinast, J., 2019. Model-based approach to the design of pharmaceutical roller-compaction processes. Int. J. Pharm. X (1), 100005. https://doi.org/10.1016/j.ijpx.2019.100005.

Train, D., 1956. An Investigation into the Compaction of Powders. J. Pharm. Pharmacol. 8, 745–760. https://doi.org/10.1111/j.2042-7158.1956.tb12206.x.

Wunsch, I., Finke, J.H., John, E., Juhnke, M., Kwade, A., 2019. A mathematical approach to consider solid compressibility in the compression of pharmaceutical powders. Pharm 11, 3. https://doi.org/10.3390/pharmaceutics11030121.

Zinchuk, A.V., Mullarney, M.P., Hancock, B.C., 2004. Simulation of roller compaction using a laboratory scale compaction simulator. Int. J. Pharm. 269 (2), 403–415. https://doi.org/10.1016/j.ijpharm.2003.09.034.